Advances in Engineering Software 120 (2018) 36–44

Contents lists available at ScienceDirect

Advances in Engineering Software

journal homepage: www.elsevier.com/locate/advengsoft

A local numerical solution of a fluid-flow problem on an irregular domain

G. Kosec*

Jožef Stefan Institute, Department of Communication Systems, Jamova 39 1000 Ljubljana, Slovenia

ARTICLE INFO

Article history:
Received 21 December 2015
Revised 7 March 2016
Accepted 16 May 2016
Available online 24 May 2016

Keywords:
Navier-Stokes
Meshless local strong form method
Local pressure-velocity coupling
Random geometry
Lid driven
Backward facing step

ABSTRACT

This paper deals with a numerical solution of an incompressible Navier-Stokes flow on non-uniform domains. The numerical solution procedure comprises the Meshless Local Strong Form Method for spatial discretization, explicit time stepping, local pressure-velocity coupling and an algorithm for positioning of computational nodes inspired by Smoothed Particles Hydrodynamics method. The presented numerical approach is demonstrated by solving a lid driven cavity flow and backward facing step problems, first on regular nodal distributions up to 315,844 (562×562) nodes and then on domain filled with randomly generated obstacles. It is demonstrated that the presented solution procedure is accurate, stable, convergent, and it can effectively solve the fluid flow problem on complex geometries. The results are presented in terms of velocity profiles, convergence plots, and stability analyses.

1. Introduction

Computational fluid dynamics (CFD) is a field of a great interest among researchers in many fields of science, e.g. studying mathematical fundaments of numerical methods, developing novel physical models, improving computer implementations, and many others. Pushing the limits of all the involved fields of science helps community to deepen the understanding of several natural and technological phenomena. Weather forecast, ocean dynamics, water transport, casting, various energetic studies, etc., are just few examples where fluid dynamics plays a crucial role. The core problem of the CFD is solving the Navier-Stokes Equation [1] or its variants, e.g. Darcy or Brinkman equation for flow in porous media. This paper focuses on a solution of the Navier-Stokes equation in a randomly generated domain with a local numerical approach.

Usually, numerical methods such as the Finite Volume Method (FVM), Finite Difference Method (FDM), or the Finite Element Method (FEM) are typically used for solving fluid flow problems. Although classical methods, especially FEM, offer several advanced features, the meshing of realistic domains still remains one of the most cumbersome and time-demanding step in the entire numerical solution process, since it often involves a significant user's assistance. In past few years the coupling of Computer Aided Design (CAD) and FEM analysis [2] alleviates that burning problem. The approach is also referred to as an isogeometric analysis and is focused on integration of FEM into conventional Non-Uniform Rational Basis Splines (NURBS) based CAD environments. On the other hand, the most intuitive and straightforward to implement is definitely the FDM approach that performs excellent as long as the treated domain can be described with an equidistant orthogonal mesh, which unfortunately covers only limited spectra of problems.

A promising alternative is a class of meshless methods (MM) that are based on scattered discretization nodes. MMs originate in the seventies with Smoothed Particles Hydrodynamics (SPH) [3] and develop further with the Diffuse Element Method (DEM), the Meshless Petrov-Galerkin method (MPG), the Element Free Galerkin method (EFG), etc. [4]. The SPH, an Eulerian kernel based approximation method, is an effective tool for simulations of problems where mesh-based method fail, for example breaking waves, gas problems and many more. However, SPH suffers from inconsistency due to the combination of Eulerian kernel and Lagrangian description of motion. The more consistent particle method with Lagrangian kernels has been later introduced for solution of solid mechanics problems [5].

In this paper, one of the simplest class of MMs, Meshless Local Strong Form Method (MLSM), a generalization of methods which are in literature also known as Diffuse Approximate Method (DAM) [6], Local Radial Basis Function Collocation Methods (LRBFCM) [7], Generalized FDM [8], Collocated discrete least squares (CDLS) meshless [9], etc., is used. Although each of the named methods poses some unique properties, the basic concept of all local strong form methods is similar, namely, to approximate treated

* Corresponding author.
E-mail address: gkosec@ijs.si

http://dx.doi.org/10.1016/j.advengsoft.2016.05.010

fields with nodal trial functions over the local support domain. The nodal trial function is then used to evaluate various operators, e.g. derivation, integration, and after all, approximation of a considered field in arbitrary position. The MLSM could easily be understood as a meshless generalization of the FDM, however much more powerful. The MLSM has an ambition to avoid using pre-defined relations between nodes and shift this task into the solution procedure. The final goal of such an approach is higher flexibility in complex domains, moving boundaries and nodal adaptivity.

There are several publications regarding adaptive MM. The h-refinement, i.e. the adaptivity in terms of adding and/or removing nodes on/from the domain has been demonstrated with the global Radial Basis Function Collocation Method [10] in solution of nearly singular Partial Differential Equations (PDE), as well as local MMs in solution of coupled Burgers' equation [11] and torsion problem [12]. The meshless r-refinement approach, where the positions of the nodes are adjusted to obtain an optimal approximation with the total number of the nodes unchanged, has been demonstrated in solution of phase field model [13]. In general, the meshless adaptivity has been thoroughly demonstrated in crack propagation problems [14–17]. An important part of the adaptivity is the error estimate that determines the nodal density that has been discussed in [11,18].

Although the meshless methods do not require any topological relations between nodes and even randomly distributed nodes could be used [19], it is well-known that using regularly distributed nodes leads to more accurate and more stable results [20–22], which is also confirmed in this paper. Therefore, despite meshless seeming robustness regarding the nodal distribution, a certain effort has to be invested into the positioning of the nodes and this paper, to some extent, deals with this problem.

The rest of the paper is organized as follows; in Section 2 the MLSM principle is explained, in Section 3 the lid driven cavity and backward facing step problems together with base elements of the solution procedure are presented, Section 4 is focused on discussion of results, and finally, paper offers some conclusions and guidelines for future work in last section.

This paper is extension of results presented on Ninth International Conference on Engineering Computational Technology [23].

2. Numerical methodology

2.1. Meshless LOCAL STRONG FORM METHOds (MLSM)

The core of MLSM presented in this paper is a local approximation of a considered field over the overlapping local support domains, i.e. in each node a considered field is approximated over a small local sub-set of neighbouring N_S nodes. The trial function is thus introduced as

$$\theta(\mathbf{p}) = \sum_{n=1}^{N_B} \alpha_n \Psi_n(\mathbf{p}), \tag{1}$$

with N_B, α_n, Ψ_n, $\mathbf{p}(p_x, p_y)$ standing for the number of basis functions, approximation coefficients, basis functions and the position vector, respectively. The type of approximation, the size of support domain, and the type and number of basis function can be general.

Although the selection of basis function Ψ_n is general, several researchers follow the results from Franke's analysis [24] and use Hardy's Multiquadrics, however in this work the monomials are used based on the results presented in [25]. The goal here is to solve a Navier-Stokes equation, i.e. a second order PDE, and to obtain non-trivial first and second derivatives a minimal basis of five monomials $(1, p_x, p_y, p_x^2, p_y^2)$ is used. Therefore, to determine corresponding coefficients at least five support nodes are required. In such setup, i.e. support domain size is the same as the number of basis functions ($N_S = N_B$), the determination of coefficients α_n simplifies to solving a system of linear equations that results from expressing Eq. (1) in all support nodes. The system can be written in vector form as

$$\boldsymbol{\theta} = \boldsymbol{\Psi}\boldsymbol{\alpha}, \tag{2}$$

where $\boldsymbol{\theta}$ stand for field values in support nodes, $\boldsymbol{\Psi}$ basis matrix ($\Psi_{ij} = \Psi_i(\mathbf{p}_j)$) and $\boldsymbol{\alpha}$ vector of coefficients. The LRBFCM that has been recently used in various problems [26, 27] uses such collocation on different sizes of support domain, depending on the problem tackled.

If the number of support nodes is higher than the number of basis functions $N_S > N_B$ Weighted Least Squares (WLS) approximation is used to solve over-determined system (2), again, constructed by expressing (1) in all support nodes. An example of such approach is DAM [6] that was originally formulated to solve fluid flow in porous media. DAM uses six monomials for basis and nine nodded support domains to evaluate first and second derivatives of physical fields required to solve problem at hand. Note that WLS with a Gaussian weighting

$$W(\mathbf{p}) = \exp\left(-\left(\frac{\|\mathbf{p}\|}{\sigma p_{\min}}\right)^2\right) \tag{3}$$

is used, where σ stands for weight parameter and $p_{\min}$ for the distance to the first support domain node.

Our goal is to apply partial operator on a considered field

$$L\theta(\mathbf{p}) = \sum_{n=1}^{N_B} \alpha_n L\Psi_n(\mathbf{p}), \tag{4}$$

where L stands for general differential operator. Considering Eq. (4) by using explicit computation of approximation coefficients $\boldsymbol{\alpha} = \boldsymbol{\Psi}^{-1}\boldsymbol{\theta}$ results in

$$L\theta(\mathbf{p}) = \sum_{n=1}^{N_B} \left(\sum_{m=1}^{N_S} \Psi_{nm}^{-1}\theta_m\right) L\Psi_n(\mathbf{p}). \tag{5}$$

Using merely few summation rules the Eq. (5) can be rewritten in a more convenient form

$$L\theta(\mathbf{p}) = \sum_{m=1}^{N_S} \chi_m^L(\mathbf{p})\theta(\mathbf{p}_m), \tag{6}$$

where the shape function χ_m^L is introduced as

$$\chi_m^L(\mathbf{p}) = \sum_{n=1}^{N_B} \Psi_{nm}^{-1} L\Psi_n(\mathbf{p}), \tag{7}$$

with $\boldsymbol{\Psi}^{-1}$standing for inverse/pseudo inverse of the approximation system matrix.

The presented formulation is convenient for implementation since most of the complex operations are performed only when nodal topology changes, i.e. when the system (2) has to be re-evaluated. In the main simulation, the pre-computed shape functions are then convoluted with the vector of values in the support to evaluate the desired operator, refer to Eq. (16) for example. The presented MLSM approach is even easier to handle than the FDM, however despite its simplicity it offers many possibilities for treating challenging cases, e.g. nodal adaptivity to address regions with sharp discontinuities or p-adaptivity to treat obscure anomalies in physical field. The stability versus computation complexity and accuracy can be regulated simply by changing number of support nodes, etc. All these features can be controlled on the fly during the simulation.

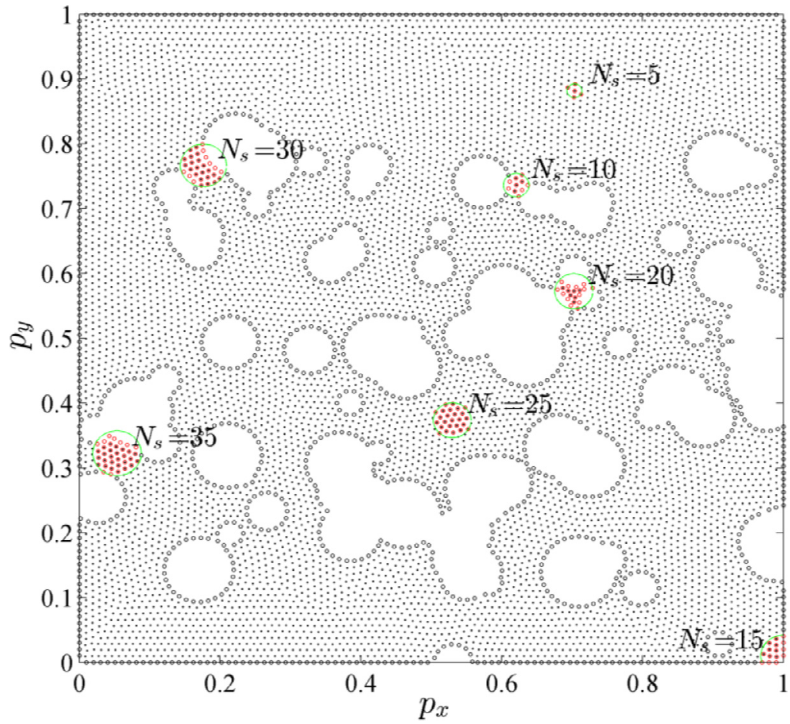

Fig. 1. Distribution of nodes within a randomly generated domain. The example support domains nodes are marked with red circles. (For interpretation of the references to colour in this figure legend, the reader is referred to the web version of this article.)

2.2. Positioning of computational nodes

To construct stable and reliable shape functions the matrix $\mathbf{\Psi}$ has to be well-conditioned. To achieve that, the support domains need to be non-degenerated [28], i.e. the distances between support nodes have to be balanced. Naturally, this condition is fulfilled in regular nodal distributions, but when working with complex geometries, the nodes have to be positioned accordingly. There are different algorithms designed to optimally fill the domain with different shapes [29,30]. However, in this paper the intrinsic feature of the MLSM is used to take care of that problem. The goal is to minimize the overall support domain degeneration in order to attain stable numerical solution. In other words, a global optimization problem with the overall deformation of the local support domains acting as the cost function is tackled. The quality of the nodal distribution is measured as

$$C = \frac{\min(\mathbf{d})}{\max(\mathbf{d})}, \tag{8}$$

where $\mathbf{d}$ stands for vector of distances between each node at its closest neighbour. We seek the global minimum by a local iterative approach. In each iteration, the computational nodes are translated according to the local derivative of the weight function

$$\delta\mathbf{p}(\mathbf{p}) = -\sigma_k \sum_{n=1}^{N_S} \nabla W(\mathbf{p} - \mathbf{p}_n), \tag{9}$$

where $\delta\mathbf{p}, \mathbf{p}_n$ and σ_k stand for the offset of the node, position of nth support node and relaxation parameter, respectively. After offsets in all nodes are computed, the nodes are repositioned as

$$\mathbf{p} \leftarrow \mathbf{p} + \delta\mathbf{p}(\mathbf{p}). \tag{10}$$

Presented iterative process procedure begins with positioning of boundary nodes, which is considered as the definition of the domain, and then followed by the positioning of internal nodes according to the Eqs. (9) and (10). In Fig. 1 the example of domain generated with presented procedure is demonstrated on rectangular domain filled with 90 randomly generated circular obstacles. The quality of nodal distribution in Fig. 1 is $C = 0.75$. Note that quality of uniform nodal distribution is $C = 1.00$. Besides nodes few support domains of different sizes are also presented.

2.3. Numerical examples

The presented numerical approach is first tested on a lid driven cavity problem that stands for a standard benchmark test for validation of the fluid flow solvers. It has been proposed in 1982 [31] and since then solved by many researchers with wide spectra of different numerical methods. The test is still widely studied and used for validation of novel methods and numerical principles, for example, recently for adaptive Finite-Volume Method [32] as well as meshless methods [33–35]. The problem is governed by following equations

$$\nabla \cdot \mathbf{v} = 0, \tag{11}$$

$$\frac{\partial \mathbf{v}}{\partial t} + \nabla \cdot (\mathbf{v}\mathbf{v}) = -\nabla P + \frac{1}{\mathrm{Re}} \nabla^2 \mathbf{v} \tag{12}$$

where $\mathbf{v}$, t, P, and Re stand for dimensionless velocity, time, pressure, and Reynolds number, respectively. Non-permeable and no-slip velocity boundaries are assumed. The lid velocity is set to 1 and initial pressure and velocity are set to zero. Problem is schematically presented in Fig. 2.

In addition to the lid driven cavity a Backward-Facing Step problem [36] is tackled to increase the confidence in the presented MLSM approach. The case is also used as a standard benchmark test [36], where the model (11) (12) is solved on an open domain with prescribed inlet velocity

$$v_x(p_y) = \frac{3}{2}\left(1 - \frac{p_y - 0.75}{0.25}\right)^2. \tag{13}$$

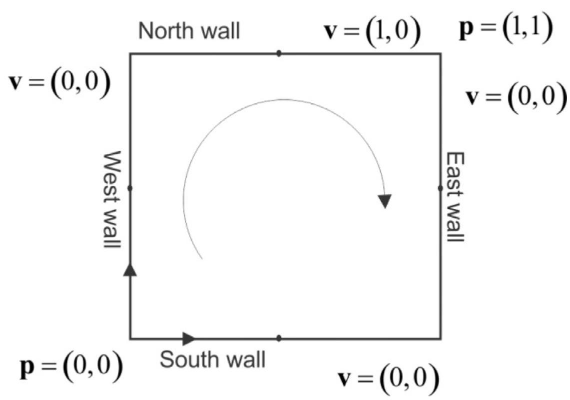

Fig. 2. Scheme of the lid driven cavity problem.

The Neumann boundary conditions for velocity components are prescribed at the outlet boundary. The problem is schematically presented in Fig. 3.

The well-known problem of solving a problem at hand is a pressure-velocity coupling. There are different approaches towards coupling Eqs. (11) and (12) [1,37]. In general, one solves a Poisson pressure or pressure correction equation [1]. In this work the local approach is preferred. A possible way to complete the task is to use the false time transient method [38] for solving a Poisson equation. An artificial time dependency is added to the Poisson equation in order to transform it to a parabolic equation that can be solved locally through explicit stepping. Another approach is to use Artificial Compressibility Method (ACM) that has been recently under intense research [39]. Although basic assumptions seem different, both approaches lead to the same coupling. With the explicit temporal discretization the problems is formulated as

$$\hat{\mathbf{v}} = \mathbf{v}_0 + \Delta t\left(-\nabla P_0 + \frac{1}{\mathrm{Re}}\nabla^2\mathbf{v}_0 - \nabla\cdot(\mathbf{v}_0\mathbf{v}_0)\right) \tag{14}$$

$$P = P_0 - \varsigma\Delta t_F\nabla\hat{\mathbf{v}} + \varsigma\Delta t_F\Delta t\nabla^2\widehat{P}_0, \tag{15}$$

where $\hat{\mathbf{v}}$, Δt, ς, Δt_F and P stand for intermediate velocity, time step, relaxation parameter, artificial time step, and pressure respectively, and $\mathbf{v}_0$ and P_0 stand for velocity and pressure from previous time step. First, the intermediate velocity is computed from previous time step (14). Second, the velocity is driven towards solenoidal field by correcting the pressure (15). Note that no special boundary conditions for pressure are used, i.e. the pressure on boundaries is computed with the same approach as in the interior of the domain. In general, the internal iteration with an artificial time step is required until the divergence of the velocity field is not below required criteria. However, if one is interested only in a steady-state solution, the internal iteration can be skipped and Δt equals Δt_F. Without internal stepping the transient of the solution is distorted by artificial compressibility effect. This approach is also known as ACM with Characteristics-based discretization of continuity equation, where the relaxation parameter relates to the artificial speed of sound [40].

The most computationally demanding parts of the code are the spatial loops, i.e. computation of new velocity and pressure correction. Spatial loops are incorporated into the temporal loop and additionally into pressure pressure-velocity coupling iteration loop, when dealing with transient problems. In each spatial loop one equation is computed. Each equation comprises different partial differential operations that are evaluated as a convolution of the corresponding shape functions and support domain values of the treated field. For example, a new iteration of pressure (15) is computed as

$$P(\mathbf{p}_n) = P_0(\mathbf{p}_n) - \varsigma\Delta t_F\underbrace{\left[\sum_{m=1}^{N_S}\chi_m^{\partial x}v_x(\mathbf{p}_m) + \sum_{m=1}^{N_S}\chi_m^{\partial y}v_y(\mathbf{p}_n)\right]}_{\nabla\cdot\mathbf{v}} + \varsigma\Delta t_F\Delta t\underbrace{\sum_{m=1}^{N_S}\chi_m^{\nabla^2}P_0(\mathbf{p}_m)}_{\nabla^2 P} \tag{16}$$

The computation takes place in all nodes. The $\boldsymbol{\chi}^{\nabla^2}$ and $\boldsymbol{\chi}^{\partial x,\,\partial y}$stand for pre-computed shape functions and its derivatives, refer to equation (7). The computation of velocity field follows the same principles.

3. Results of numerical integration

3.1. Comparison with published data and convergence analysis

First the lid driven cavity problem is solved. At low Re numbers one global vortex appear approximately at the centre of the domain. With increasing Re the complex structure of eddies near cavity corners evolve. The present MLSM solution of the problem is compared at three different Re = [100,1000,3200] numbers against three different solutions, namely, *Mramor* [33], *Sahin* [41] and *Ghia* [42]. In Fig. 4 comparison of MLSM and *Mramor* in terms of mid-plane velocity profile $v_y(p_x, 0.5)$ is presented together with a MLSM contour plot of velocity magnitude for Re = 3200 case.

Results, presented in Fig. 4, are computed on a regularly distributed N=22,801 (151 × 151) nodes with support domain of size 5, time step $0.5 \cdot 10^{-4}$, and relaxation parameter set to 1. In Fig. 5 more precise spatial convergence in terms of maximal v_y on a range from N = 121 (11 × 11) to N = 315,844 (562 × 562) uniformly distributed nodes is demonstrated. It can be seen that the Re = 3200 case cannot be computed with less than N = 6561 (81 × 81) nodes, otherwise, the results converge towards reference solutions. Note that the reference solutions do not represent the convergence behaviour and are added only for the sake of comparison. The tabular form of results is presented in Table 1. It can

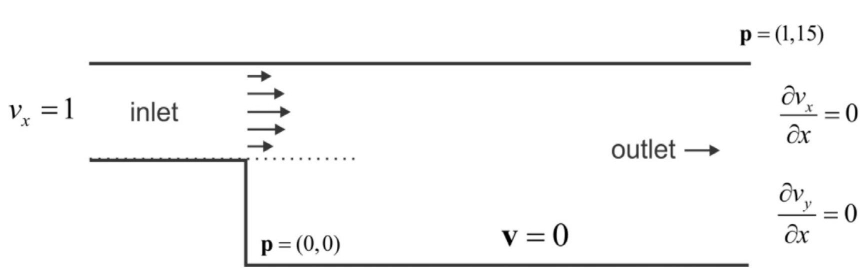

Fig. 3. Scheme of the Backward-Facing Step problem.

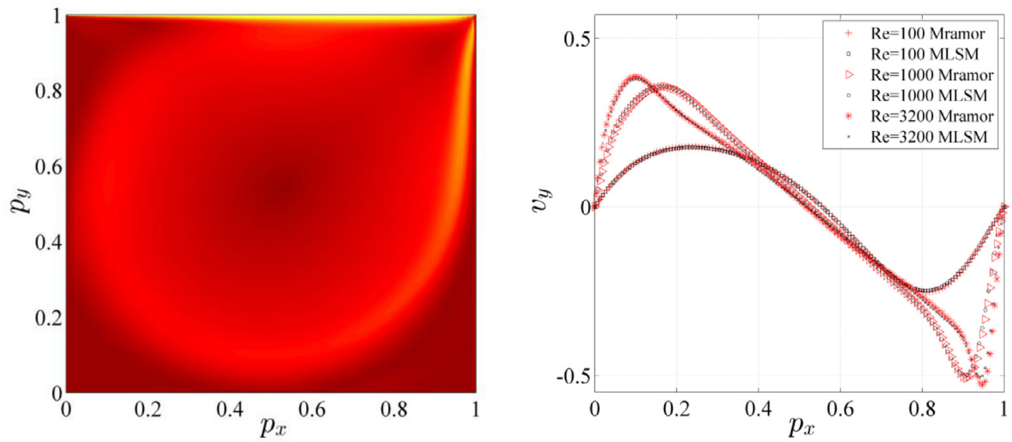

Fig. 4. Contour plot of velocity magnitude for Re=3200 (left) and comparison of horizontal mid-plane velocity profile $v_y(p_x, 0.5)$ against recently published solution *Mramor*.

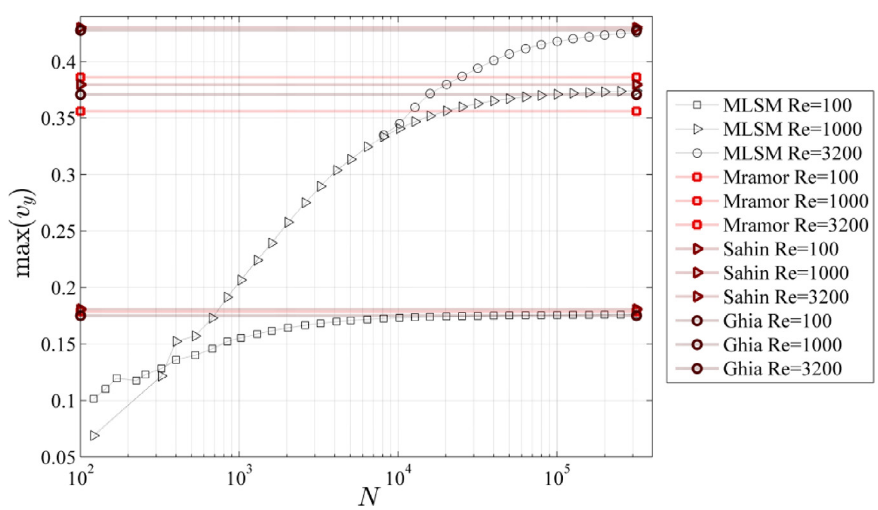

Fig. 5. The maximal mid-plane velocity $\max(v_y(p_x, 0.5))$ with respect to the number of computational nodes for different Re numbers. Blue, black and green lines stand for reference solutions *Mramor, Sahin* and *Ghia*, respectively. (For interpretation of the references to colour in this figure legend, the reader is referred to the web version of this article.)

Table 1
Tabular comparison of MLSM against reference solutions in terms of positions and values of maximal and minimal v_y mid-plane velocities(p_x, v_y).

RE	MLSM	Mramor	Sahin	Ghia
$\max(v_y)$				
100	(0.2367, 0.1790)	(0.2379, 0.1788)	(0.2354, 0.1809)	(0.2344, 0.1752)
1000	(0.1584, 0.3754)	(0.1665, 0.3560)	(0.1573, 0.3769)	(0.1563, 0.3709)
3200	(0.0961, 0.4270)	(0.1000, 0.3861)	(0.0972, 0.4324)	(0.0938, 0.4276)
$\min(v_y)$				
100	(0.8096, -0.2524)	(0.8102, -0.2526)	(0.8127, -0.2560)	(0.8047, -0.2453)
1000	(0.9093, -0.5233)	(0.9070, -0.5082)	(0.9087, -0.5284)	(0.9100, -0.5263)
3200	(0.9466, -0.5526)	(0.9471, -0.5290)	(0.9491, -0.5691)	(0.9453, -0.5405)

be seen that MLSM agree well with *Sahin* and *Ghia* while *Mramor* deviate a bit more. From Fig. 4, Fig. 5 and Table 1 it can be concluded that the presented MLSM methodology provides accurate, convergent and stable results.

To increase confidence into the MLSM solution procedure additional tests are performed on a backward-facing step problem. In Fig. 6 the MLSM solution of the backward-facing step problem at $\mathrm{Re} = 800$ on 6615 uniformly distributed nodes is presented in terms of velocity magnitude contour plot. Note that although the computation is done for $p_x = [0, 15]$ figure is, for the sake of better presentation, limited to $p_x = [0, 10]$. Furthermore, on Fig. 7 a comparison of vertical velocity profiles solved by MLSM and reference data [36] is presented.

3.2. Computations on irregular nodal distributions

Next analysis is focused on the impact of support domain deformation on the computation efficiency. To test MLSM behaviour, a randomized nodal distribution is used, i.e. the initially uniformly distributed nodes are translated by random offsets

$$\mathbf{p}_i \leftarrow \mathbf{p}_i + D\mathbf{r}\Delta p, \tag{17}$$

where $\mathbf{r} = (r_x, r_y)$ is vector of random numbers within $[-1, 1]$, D is deformation magnitude, $\mathbf{p}_i$ is position of ith node, and Δp is spatial step of original uniform nodal distribution. In Fig. 8 contour plots of maximal horizontal cross-section velocity computed on $N_D = 10^4$ nodes with respect to the deformation magnitude and

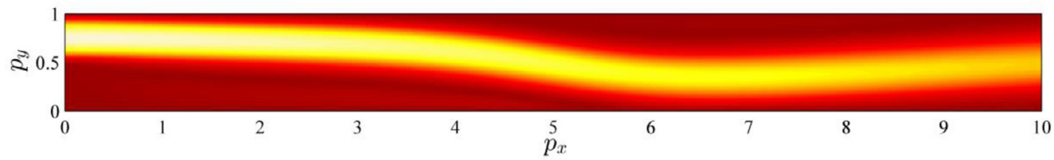

Fig. 6. Velocity magnitude contour plot for backward-facing step problem.

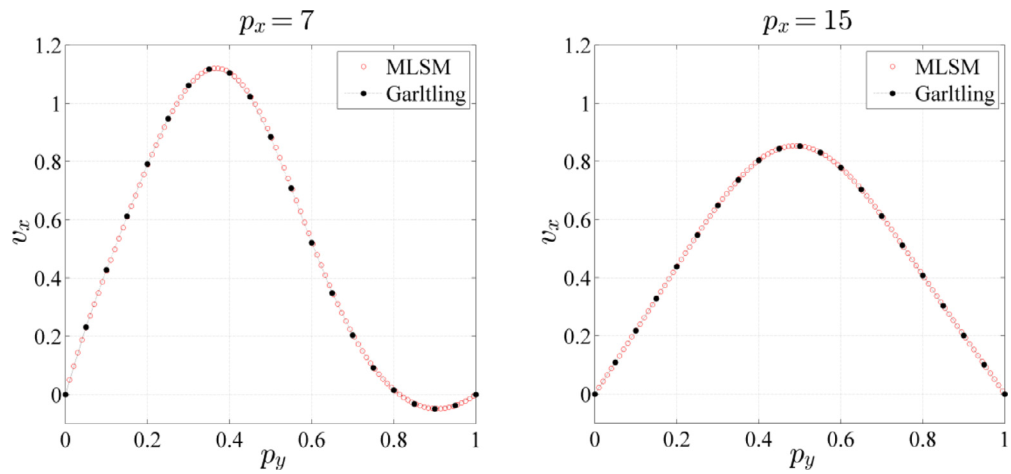

Fig. 7. Comparison of vertical velocity profiles at $p_x = 7$ and $p_x = 15$ for backward-step facing problem.

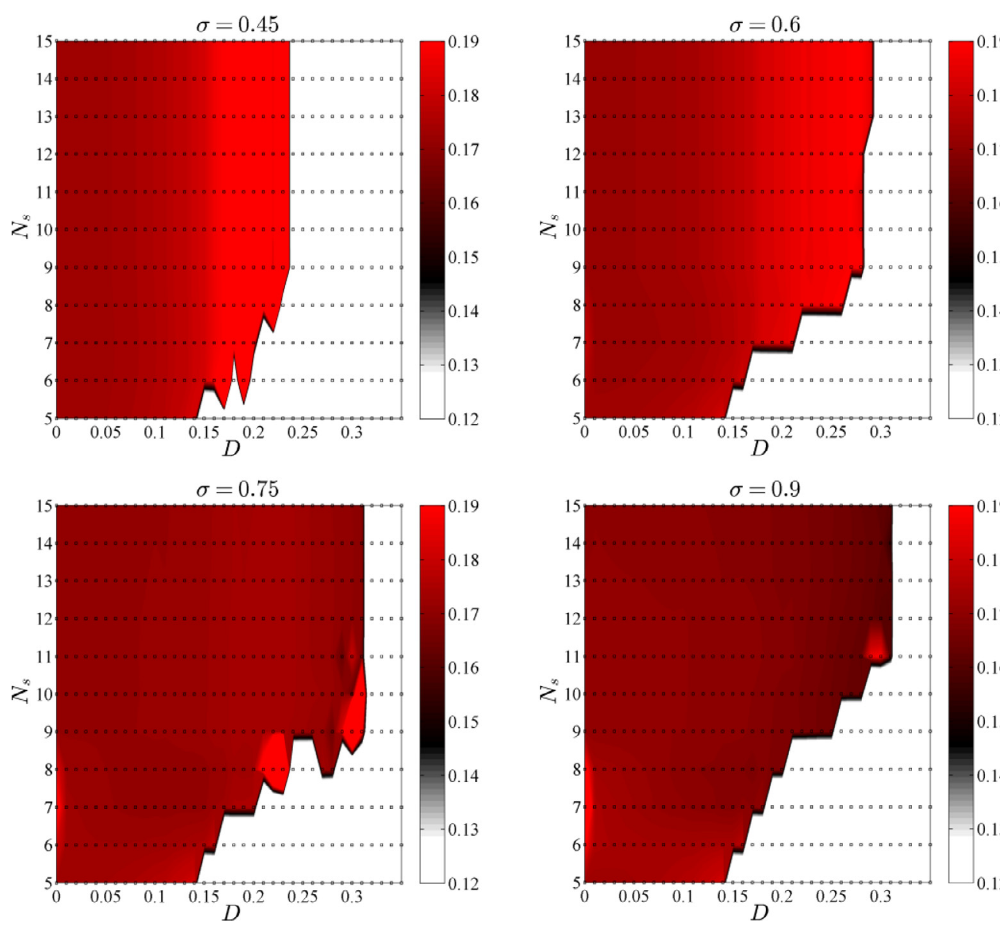

Fig. 8. The maximal horizontal cross-section velocity with respect to deformation magnitude and number of support nodes for different weight parameters.

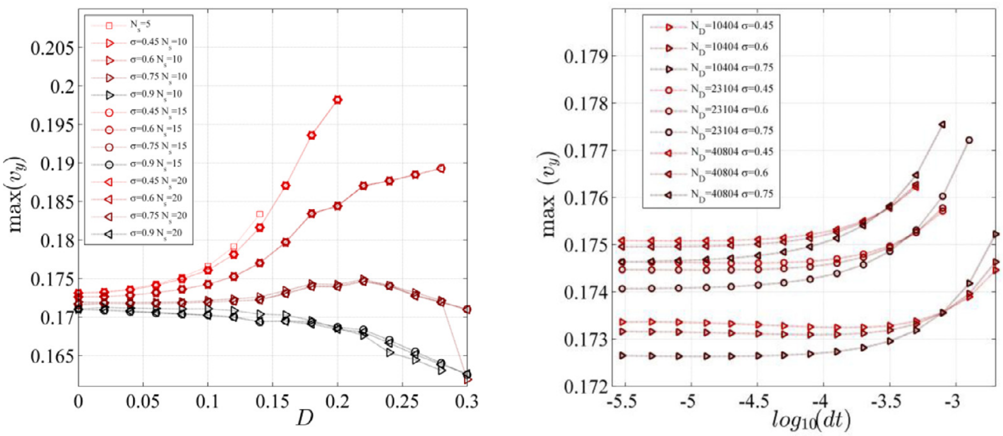

Fig. 9. The impact of nodal deformation on the performance of the method with respect to the support domain size and weight parameter (left) and the impact of the time step, weight parameter and number of computational nodes on the results (right).

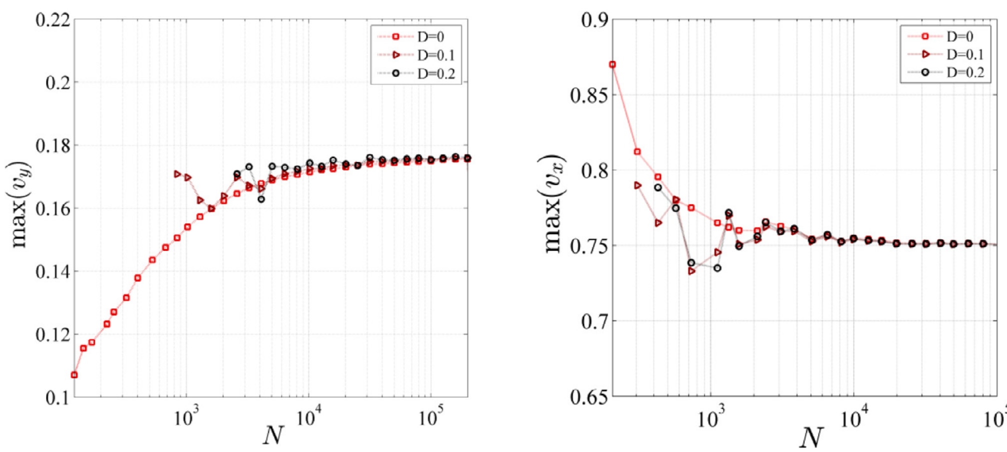

Fig. 10. max($v_y(p_x$, 0.5))for lid driven problem (left) and max($v_x(p_x$, 7))for backward facing step problem (right) with respect to the number of nodes and deformation of nodal distribution.

number of support nodes for different weight parameters is presented.

It can be clearly seen that increasing the deformation gravely affects the results, especially; when the support is small, i.e. small number of nodes influences the approximation function, as a consequence of a small number of support nodes and/or the small weight parameter. With a small support domain MLSM starts to diverge already at deformation $D = 0.1$. Increasing the support, i.e. increasing the weight parameter as well as number of support nodes, improves results. Fig. 8 serves mainly to determine the stability limit for given setup, where the instable setups are represented with zero values, shown as white areas on the figure. More quantitative representation of phenomenon is presented in Fig. 9, where it can be also seen that the wider supports result in a lower velocities due to the fact that WLS approximation with wide support domains fails to capture all the details in the field, which introduces additional approximation error. The impact of the time step on results for different discretizations and weight parameters with $N_S = 15$ is also presented in Fig. 9, where the stability limit due to the explicit stepping can be clearly seen.

The number of support nodes influences the computational time since the generation of shape functions can be estimated to complexity $O(N_s^3)$ and the evaluation of partial operators to $O(N_s)$. In many practical cases, when temporal loop presents majority of the execution time, the construction of shape function can be considered as a pre-process. In such cases the execution time and memory consumption are linearly dependant on the support size.

From above results a general conclusion can be drawn, namely, increasing the support domain stabilizes the MLSM with respect to the nodal deformation, at the cost of accuracy and computational complexity. Ultimately, a setup with $\sigma = 0.75$ and support size of 15 nodes is chosen as a reasonable trade-off between stability, accuracy and computation cost that provides stable results on nodal distribution up to $D = 0.3$ that corresponds to the $C = 0.54$.

To finally confirm the MLSM performance convergence plots for lid driven cavity and BFS problems at $\mathrm{Re} = 100$ are presented for regular and irregular nodal distributions in Fig. 10. We can see that for both problems MLSM shows convergent behaviour. It can be also seen that, when working with low number of nodes, irregularity of nodal distribution destabilizes computations. However, the problem diminishes with increasing the number of nodes. For both problems approximately 10^4 nodes suffices for stable solution on regular as well as irregular nodal distributions.

Previous analyses confirmed that MLSM with support size 15 is stable up to $C = 0.54$ and that we can build a nodal distribution within a randomly generated domain with C of order 0.75. Although the quality of generated domain depends on the input geometry, the difference between the stability limit and the quality of the generated domain is high enough for practical computations. This is confirmed by applying the presented methodology on lid driven cavity problem in different irregular domains. In Fig. 11 solution of a $\mathrm{Re} = 1000$ case problem solved in domain filled with uniformly distributed circular obstacles and in Fig. 12 in domain filled with randomly distributed circular obstacles are presented.

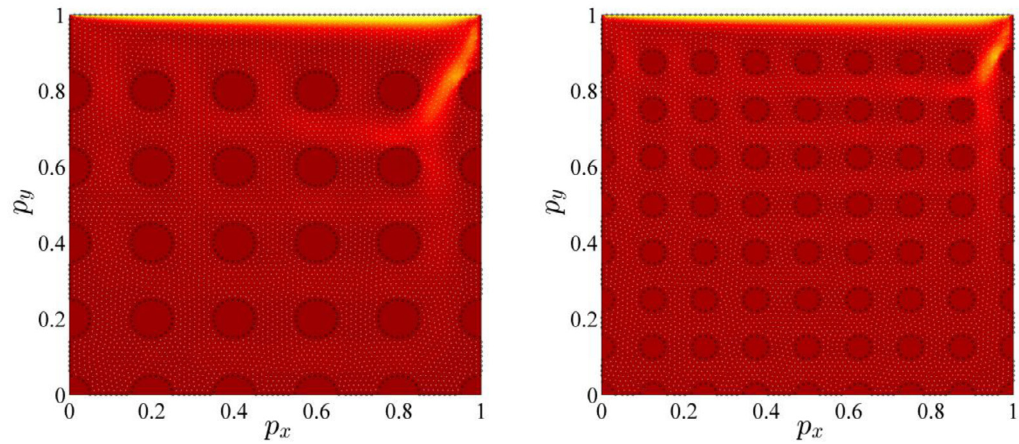

Fig. 11. Solution of lid driven problem in a domain filled with uniformly distributed circular obstacles: left 30 obstacles, right 72 obstacles.

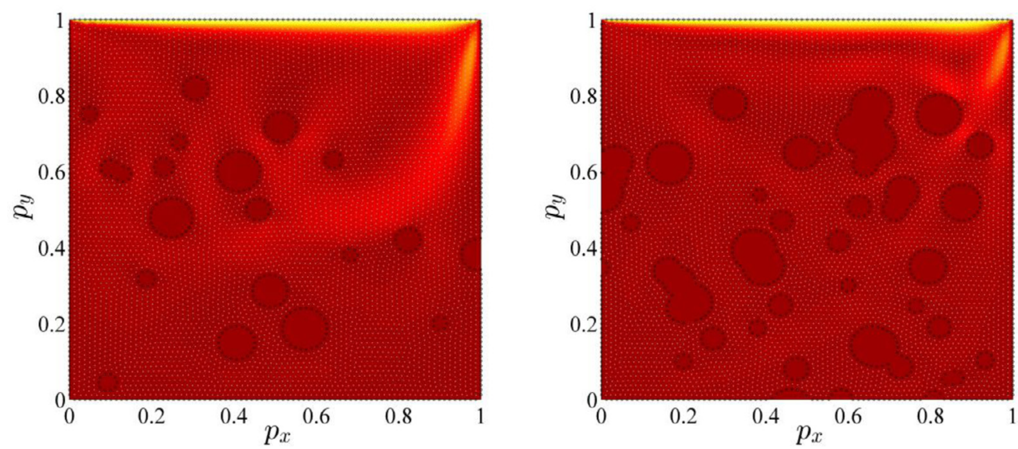

Fig. 12. Solution of lid driven problem in a domain filled with randomly distributed circular obstacles: left 20 obstacles, right 50 obstacles.

On all figures computational nodes are marked with white dots, boundary nodes with black dots while velocity field is represented with velocity magnitude contour plot.

4. Conclusions

In this paper it is demonstrated that MLSM coupled with a local pressure-velocity, and a local nodal positioning algorithm can effectively solve Navier Stokes problem in complex domains. The solution procedure is first tested on an uniform domain for lid driven cavity problem at $Re = [100,1000,3200]$ with good agreement with published data as well as good convergence achieved. The solution procedure is further tested also on backward facing step problem at $Re = 800$, again good agreement with published data is demonstrated. The numerical approach is finally applied on the domain filled with randomly generated holes. It is demonstrated that presented MLSM with five monomials and support size of 15 with WLS used for construction of shape functions can effectively solve such problems. This conclusion is supported with several analyses.

The complete locality of the introduced numerical scheme has several beneficial effects. One of the most attractive is the simplicity since it could be understood as a generalized FDM method. The presented methodology is relatively simple to understand and implement, which makes it potentially powerful tool for engineering simulations. Besides simplicity and straightforward implementation, there are many opportunities to fully exploit modern computer architectures through different parallel computing strategies [25, 43–46]. More detailed comparison of MLSM, FEM and FDM also in context of implementation and parallel execution performances can be found in [20].

Future work will be focused on implementation of more complex physical models, more detailed analysis of MLSM application on complex 3D domains.

Acknowledgment

The author acknowledges the financial support from the state budget by the Slovenian Research Agency under Grant P2-0095.

References

[1] Ferziger JH, Perić M. Computational methods for fluid dynamics. Berlin: Springer; 2002.
[2] Cottrell JA, Hughes JRT, Bazilevs Y. Isogeometric analysis: toward integration of CAD and FEA 2009.
[3] Gingold RA, Monaghan JJ. Smoothed particle hydrodynamics: theory and application to non-spherical stars. Mon Not Roy Astron So 1977;181:375–89.
[4] Li S, Liu KW. Meshfree and particle methods and their applications. Appl Mech Rev 2002;55:1–34.
[5] Rabczuk T, Belytschko T, Xiao SP. Stable particle methods based on Lagrangian kernels. Comput Method Appl M. 2004;193:1035–63. doi:10.1016/j.cma.2003.12.005.
[6] Wang CA, Sadat H, Prax C. A new meshless approach for three dimensional fluid flow and related heat transfer problems. Comput Fluids 2012;69:136–46. doi:10.1016/j.compfluid.2012.08.017.
[7] Šarler B. From global to local radial basis function collocation method for transport phenomena. Springer: Advances in Meshfree Techniques. Berlin; 2007. p. 257–82.
[8] Yang C, Tang D, Yuan C, Kerwin W, Liu F, Canton G, et al. Meshless generalized finite difference method and human carotid atherosclerotic plaque progression simulation using multi-year MRI patient-tracking data. CMES-Comp Model Eng 2008;28:95–107.

[9] Arzani H, Afshar MH. Solving Poisson's equation by the discrete least square meshless method. WIT Trans Model Simul 2006;42:23–31.
[10] Libre AL, Emdadi A, Kansa EJ, Shekarchi M, Rahimian M. A fast adaptive wavelet scheme in RBF collocation for nearly singular potential PDEs. CMES–Comp Model Eng 2008;38:263–84.
[11] Kosec G, Šarler B. H-adaptive local radial basis function collocation meshless method. CMC-Comput Mater Con 2011;26:227–53.
[12] Liu GRK, T BB, Lu C. A stabilized least-squares radial point interpolation method (LS-RPCM) for adaptive analysis. Comput Meth Appl Mech Eng 2006;195:4843–61.
[13] Kovačević I, Šarler B. Solution of a phase-field model for dissolution of primary particles in binary aluminum alloys by an r-adaptive mesh-free method. Mater Sci Eng 2005;A413-414:423–8.
[14] Rabczuk, T, Belytschko, T. An adaptive continuum/discrete crack approach for meshfree particle methods. Engineering 2003.
[15] Rabczuk T, Samaniego E. Discontinuous modelling of shear bands using adaptive meshfree methods. Comput Method Appl M 2008;197:641–58.
[16] Rabczuk T, Belytschko T. Adaptivity for structured meshfree particle methods in 2D and 3D. Int J Numer Meth Eng 2005;63:1559–82.
[17] Rabczuk T, Belytschko T. A three-dimensional large deformation meshfree method for arbitrary evolving cracks. Comput Method Appl M 2007;196:2777–99. doi:10.1016/j.cma.2006.06.020.
[18] Amani J, Saboor Bagherzadeh A, Rabczuk T. Error estimate and adaptive refinement in mixed discrete least squares meshless method. Math Prob Eng 2014;2014:1–16 Article ID 721240, 16 pages. doi:10.1155/2014/721240.
[19] Reuther K, Sarler B, Rettenmayr M. Solving diffusion problems on an unstructured, amorphous grid by a meshless method. Int J Therm Sci. 2012;51:16–22. doi:10.1016/j.ijthermalsci.2011.08.017.
[20] Trobec R, Kosec G. Parallel scientific computing : theory, algorithms, and applications of mesh based and meshless methods. Springer Cham Heidelberg New York Dordrecht London: Springer; 2015.
[21] Trobec R, Kosec G, Šterk M, Šarler B. Comparison of local weak and strong form meshless methods for 2-D diffusion equation. Eng Anal Bound Elem 2012;36:310–21.
[22] Amani J, Afshar MH, Naisipour M. Mixed discrete least squares meshless method for planar elasticity problems using regular and irregular nodal distributions. Eng Anal Bound Elem 2012;36:894–902. doi:10.1016/j.enganabound.2011.09.012.
[23] Kosec G. Meshless solution of incompressible flows in complex domains. In: Iványi P, Topping BHV, editors. Proceedings of the ninth international conference on engineering computational technology. Stirlingshire, United Kingdom: Civil-Comp Press; 2014 doi:10.4203/ccp.105.75, paper 75.
[24] Franke J. Scattered data interpolation: tests of some methods. Math Comput 1982;48:181–200.
[25] Kosec G, Zinterhof P. Local strong form meshless method on multiple graphics processing units. CMES-Comp Model Eng 2013;91:377–96.
[26] Kosec G, Trobec R. Simulation of semiconductor devices with a local numerical approach. Eng Anal Bound Elem 2015;50:69–75.
[27] Kosec G, Šarler B. Simulation of macrosegregation with mesosegregates in binary metallic casts by a meshless method. Eng Anal Bound Elem 2014;45:36–44.
[28] Lee CK, Liu X, Fan SC. Local muliquadric approximation for solving boundary value problems. Comput Mech 2003;30:395–409.
[29] Löhner R, Oñate E. A general advancing front technique for filling space with arbitrary objects. Int J Numer Meth Eng 2004;61:1977–91.
[30] Liu Y, Nie Y, Zhang W, Wang L. Node placement method by bubble simulation and its application. CMES-Comp Model Eng 2010;55:89.
[31] Ghia U, Ghia K, Shin C. High-re solutions for incompressible flow using the Navier-Stokes equations and a multigrid method. J Comput Phys 1982;48:387–411.
[32] Magalhães JPP, Albuquerque DMS, Pereira JMC, Pereira JCF. Adaptive mesh finite-volume calculation of 2D lid-cavity corner vortices. J Comput Phys 2013;243:365–81.
[33] Mramor K, Vertnik R, Šarler B. Low and intermediate re solution of lid driven cavity problem by local radial basis function collocation method. CMC-Comput Mater Con 2013;1:1–21.
[34] Bustamante CA, Power H, Sua YH, Florez WF. A global meshless collocation particular solution method (integrated Radial Basis Function) for two-dimensional Stokes flow problems. Appl Math Model 2013;37:4538–47.
[35] Bourantas GC, Loukopoulos VC. A meshless scheme for incompressible fluid flow using a velocity–pressure correction method. Comput Fluids 2013;88:189–99.
[36] Gartling DK. A test problem for outflow boundary conditions—flow over a backward-facing step. Int J Numer Meth Fl 1990;11:953–67.
[37] Johnston H, Liu JG. Accurate, stable and efficient Navier–Stokes solvers based on explicit treatment of the pressure term. J Comput Phys 2004;199:221–59.
[38] Lee TS. A false transient approach to steady state solution of fluid flow through vascular constrictions. Comput Mech 1991;7:269–77.
[39] Arpino F, Massarotti N, Mauro A, Nithiarasu P. Artificial compressibility based CBS solutions for double diffusive natural convection in cavities. Int J Numer Method H 2013;23:205–25.
[40] Rahman MM, Siikonen T. An artificial compressibility method for viscous incompressible and low Mach number flows. Int J Numer Meth Eng 2008;75:1320–40.
[41] Sahin M, Owens R. A novel fully implicit finite volume method applied to the lid-driven cavity problem. Part I: high Reynolds number flow calculations. Int J Numer Meth Fl. 2003;42:57–77.
[42] Ghia U, Ghia K, Shin C. High-Re solutions for incompressible flowusing the Navier-Stokes equations and a multigrid method. J Comput Phy 1982;48:387–411.
[43] Šterk M, Trobec R. Meshless solution of a diffusion equation with parameter optimization and error analysis. Eng Anal Bound Elem 2008;32:567–77.
[44] Kosec G, Depolli M, Rashkovska A, Trobec R. Super linear speedup in a local parallel meshless solution of thermo-fluid problems. Comput Struct 2014;133:30–8. doi:10.1016/j.compstruc.2013.11.016.
[45] Trobec R, Šterk M, Robič B. Computational complexity and parallelization of the meshless local Petrov-Galerkin method. Comput Struct 2009;87:81–90.
[46] Rabczuk T, Eibl J. Simulation of high velocity concrete fragmentation using SPH/MLSPH. Int J Numer Meth Eng 2003;56:1421–44.